Shock-induced phase transition and spalling characteristic in pure iron and FeMnNi alloy*

Chen Yong-Tao(陈永涛)†, Tang Xiao-Jun(唐小军), and Li Qing-Zhong(李庆忠)

Laboratory for Shock Wave and Detonation Physical Research, Institute of Fluid Physics, China Academy of Engineering Physics, Mianyang 621900, *China*

(Received 19 October 2009; revised manuscript received 25 November 2009)

This paper provides an investigation of the phase transition and spalling characteristic induced during shock loading and unloading in the pure iron and the FeMnNi alloy. The impact for the pure iron is symmetric and with the same-thickness for both the flyer and the target plate. It is found that an abnormal multiple spalling happens in the pure iron sample as the pressure exceeds the $\alpha-\varepsilon$ transition threshold of 13 GPa. In the symmetric and same-thickness impact and reverse impact experiments of the FeMnNi alloy, two abnormal tension regions occur when the pressure exceeds the $\alpha-\varepsilon$ transition threshold of 6.3 GPa, and the reverse phase transition $\varepsilon-\alpha$ begins below 4.2 GP. The experimental process is simulated successfully from the non-equilibrium mixture phase and Boettger's model. Such abnormal spalling phenomena are believed to relate to the shocked $\alpha-\varepsilon$ phase transition. The possible reasons for the abnormal multiple spalling, which occurs during the symmetric and same-thickness impact experiments of pure iron and FeMnNi alloy, are discussed.

Keywords: pure iron, FeMnNi alloy, phase transition, spalling behaviour
PACC: 6470, 6250, 6220M

1. Introduction

Since the discovery of the $\alpha-\varepsilon$ polymorphic phase transition at high pressure in pure iron and steel by Bancroft *et al.*[1] in 1956, a great number of investigations have been reported theoretically and experimentally. This structural transition in pure iron during shock compression was inferred at a pressure of about 13 GPa and further confirmed based on the shock wave profile measurements.[2−13] Very recently, the direct observation of the $\alpha-\varepsilon$ transition in shock-compressed iron has been conducted via nanosecond x-ray diffraction, and the result is in good agreement with NEMD (none-equilibrium molecular dynamics) simulation.[14,15] Nevertheless, these studies are all about the phase transition properties or spalling behaviour, but littlie about the phase transition effects on its tensile spalling behaviour. Recently, Tang *et al.*[7,16,17] have reported an investigation of the shock-induced phase transition and spallation in pure iron and FeMnNi alloy. They found that the unique multiple and shallow spallations may occur in the shocked pure iron and FeMnNi sample when the pressure is higher than that of the phase transition, and it is proposed that such a phenomenon is related to the phase transition of the material.

This work presents further experimental measurements on the shock-induced phase transition and spalling behaviour of pure iron and FeMnNi alloy under high speed impact conditions. Employing the non-equilibrium mixture phase and Boettger model,[18] we explained the physical process associated in the non-equilibrium mixture phase transition and its effect on the dynamic tensile spall.

2. Material and method

FeMnNi alloy with the single α phase and nominal composition (mass. %): 85.03%Fe, 7.63%Mn, 7.01%Ni and 0.30%Al, and pure iron, were used in this study. The shock compression tests were performed in a 100 mm diameter light gas gun, and two kinds of impact set-ups were applied. One is referred to as the symmetric and same-thickness impact. Another is the reverse impact, in which the flyer impacts directly on a sapphire window sprayed with an aluminum membrane of 0.5 μm thickness on the impact surface. This thin aluminum membrane ensures the

*Project supported by the National Science Foundations of China (Grant Nos. 10776032 and 10902102) and Science Foundation of China Academy of Engineering Physics (Grant Nos. 20060104 and 2009B0201014).
†Corresponding author. E-mail: cythit@yahoo.cn
© 2010 Chinese Physical Society and IOP Publishing Ltd

reflection of incident laser light for measuring particle velocity. In addition, due to the quite small thickness of the aluminum membrane relative to the specimen, it is negligible in the experimental result analysis.

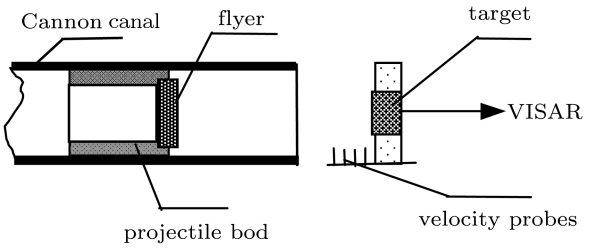


Fig. 1. The experimental configuration for shock impact test. The target is pure iron or FeMnNi alloy in the symmetric and same-thickness impact set-up, and the target is sapphire window in the reverse impact set-up.

In the two kinds of set-ups, the particle velocity at either the impact interface or the free surface was detected by a double-sensitivity velocity interferometer system for any reflector (VISAR) (100 (m/s)/fringe and 250 (m/s)/fringe). The experimental configuration is schematically shown in Fig. 1, and the material parameters are listed in Table 1, and the experimental conditions are shown in Table 2.

Table 1. Parameters of the materials.

material	$\rho_0/(\mathrm{g/cm^3})$	$C_0/(\mathrm{km/s})$	λ
pure iron	7.87	4.63	1.33
FeMnNi	7.85	4.65	1.53
sapphire	3.95	11.19	1.0

where ρ_0 is the initial density, and C_0 and λ are Hugoniot parameters of pure iron or FeMnNi alloy for the low pressure α phase.

Table 2. Parameters for experimental conditions.

test method No.	impact velocity/(m/s)	flyer/(mm×mm)	sample/(mm×mm)	window/(mm×mm)
1	848	Fe Ø95×6.3	Fe Ø95×6.3	
2	455	Fe Ø95×6.3	Fe Ø95×6.3	
3	613	FeMnNi Ø95×6	FeMnNi Ø95×6	
4	596	FeMnNi Ø95×2		sapphire Ø50×20

3. Phase transition model

According to the models proposed by Refs. [18]–[20], the following equations can be established for a material in which the phase transition occurs

$$\begin{aligned} v &= (1-\eta)v_1 + \eta v_2, \\ E &= (1-\eta)E_1 + \eta E_2, \\ S &= (1-\eta)S_1 + \eta S_2, \end{aligned} \tag{1}$$

where, η is the mass fraction of the second phase, v, E and S are specific volume, specific internal energy and specific entropy, respectively. And the subscripts 1 and 2, represent the first α and the second ε phase.

We use Boettger model[18] Eqs. (2) and (3) to describe the phase transition metastable surface and the reverse phase transition metastable surface in pure iron and FeMnNi alloy, respectively.

$$\eta_{\mathrm{mf}} = 1 - \exp[(A_{\mathrm{f}} - \Delta G)/B_{\mathrm{f}}], \tag{2}$$

$$\eta_{\mathrm{mr}} = \exp[(\Delta G - A_{\mathrm{r}})/B_{\mathrm{r}}], \tag{3}$$

where η_{mf} and η_{mr} are the mass fractions of ε phase for the metastable state. $\Delta G = G_1 - G_2$, with G_1 and G_2 the Gibbs free energies for α phase and ε phase, respectively. In the two phases mixture region, the Hugoniot lies well above the equilibrium surface defined by $G_1 = G_2$, A_{f}, B_{f}, A_{r} and B_{r} are parameters of the material.

4. Results and discussion

4.1. Phase transition properties

The free surface velocity profiles of the samples are shown in Fig. 2. In experiment No. 1, it is composed of an elastic wave E, a plastic wave P1 and a phase transition wave P2, and the phase transition $\alpha - \varepsilon$ occurs in the pure iron sample. In experiment No. 2, it is composed of an elastic wave E and a plastic wave P1, and no phase transition occurs in the pure iron sample. In experiment No. 3, it is composed of an elastic wave E, a plastic wave P1, a phase transition wave P2 and the phase interface reflection (PIR) wave, and the phase transition $\alpha - \varepsilon$ also occurs in the FeMnNi alloy sample.

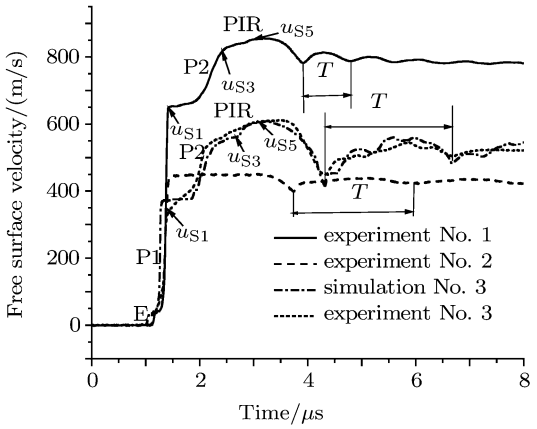


Fig. 2. Free surface velocity profile of samples. The solid line, the dashed line and the dash-dot line are the measuring signals by means of VISAR in experiments No. 1, No. 2, and No. 3, respectively. The dot line is the numerical simulation result in experiment No. 3. u_{S1}, u_{S3} and u_{S5} are the free surface velocity after P1, P2 and PIR wave, respectivelies. And T is the oscillation period.

For the experiments No. 1 and No. 3, the stress at the top of the P1 wave is identified with the onset of the phase change because it signifies a sudden increase in compressibility. In order to obtain the stress and relative volume at the phase transition, one must use the Hugoniot relations

$$\Delta\sigma = \rho_0 D \Delta u_\mathrm{p}, \quad \Delta V/V_0 = -\Delta u_\mathrm{p}/D, \tag{4}$$

$$D = C_0 + \lambda u_\mathrm{p}, \tag{5}$$

here $\Delta\sigma$ is the change in stress carried by the wave, u_p is the particle velocity, Δu_p is the change in particle velocity carried by the wave, D is the Lagrangian wave velocity, V_0 is the initial volume ($V_0 = 1/\rho_0$) and ΔV is the change in volume carried by the wave. The particle velocity u_p is assumed to be one-half of the free surface velocity u_S. The Eq. (4) was applied first to the elastic precursor and then to the P1 wave to obtain the stress and volume at the top of the P1 wave. The results are listed in Table 3.

Table 3. Summary of experiments. Velocity in km/s, stress in GPa.

No.	σ_P	V/V_0	u_{S1}	D_{p1}	σ_t	u_{S3}	D_{p2}	u_pr	σ_n	σ_r	u_{S5}	σ_s	δ_i	δ_r	δ_w
#1	14.8	0.90	0.649	5.06	12.9	0.85	2.64	–	9.8	2.5	–	–	2.0	2.0	2.0
#2	8.8	0.95	0.449	4.93	–	–	–	–	–	–	–	–	–	–	–
#3	11.1	0.89	0.35	4.9	6.3	0.59	3.8	–	–	4.8	0.6	0.3	–	–	–
#4	11.3	0.89	–	–	–	–	–	0.095	4.2	–	–	–	–	–	–

Here, σ_P is the shock peak stress, V/V_0 is the final volume compression ratio, D_{p1} is the plastic wave velocity, σ_t is the stress of the phase transition, D_{p2} is the phase wave velocity, u_pr is the interface particle velocity at which the reverse phase transition begins, σ_n is the stress of the reverse phase transition, σ_r is the stress behind the $\mathrm{P2^R}$ wave, and σ_s is the stress behind the PIR wave. δ_i is the width of the spall piece near the impact surface, which is obtained from the recovered sample. δ_r is the width of the spall piece near the free surface, which is obtained from the recovered sample. δ_w is the width of the spall piece near the free surface, which is calculated through the free surface velocity.

Referring to Figs. 3 and 4, for experiments No. 1 and No. 3, at time t_1 the plastic wave P1 reaches the free surface (the impact time of the flyer and the sample is assumed zero), in which the free surface velocity is about u_{S1}, and the sample transforms to the ε phase or $\alpha+\varepsilon$ mixed phase via the phase transition wave P2. Due to the low magnitude of the elastic wave, it has been omitted in Figs. 3 and 4. The right going plastic wave P1 reflects at the free surface and travels as a rarefaction wave R1 back into the sample, and the stress of the material behind the rarefaction wave R1 is zero. Further more, this rarefaction wave R1 encounters the oncoming phase transition wave P2 at coordinates (h_2, t_2), and the residue of the rarefaction wave R1 ($\mathrm{R1^R}$ wave) is traveling into ε-phase (or $\alpha+\varepsilon$ phase) zone and reducing the stress. At time t_3, the oncoming residue of the P2 wave reaches and reflects from the free surface, in which the free surface velocity is about u_{S3}. The material next to the free surface through which the $\mathrm{P2^R}$ wave is now traveling has never experienced a stress above the phase transition stress, and thus it remains in α phase.

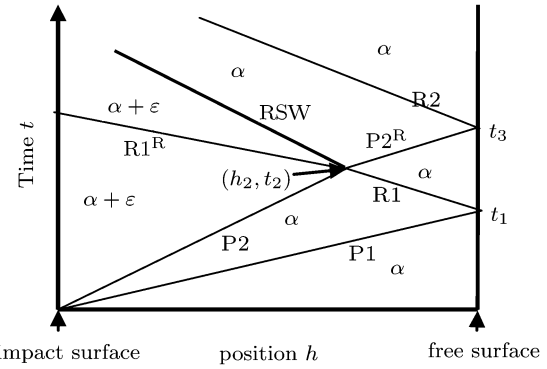


Fig. 3. Schematic wave interaction in experiment No. 1, in which the horizontal axis represents the pure iron sample thickness and the vertical axis represents time.

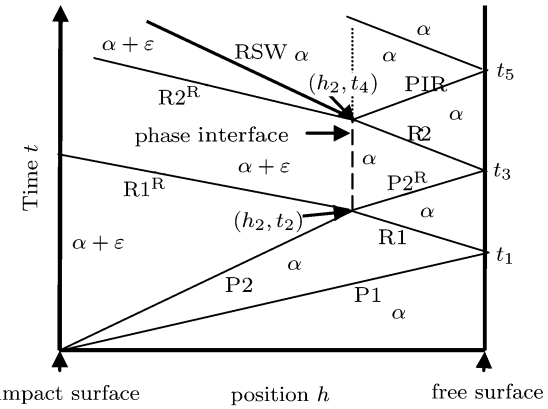


Fig. 4. Schematic wave interaction in experiment No. 3, in which the horizontal axis represents the FeMnNi sample thickness and the vertical axis represents time.

In addition, the $\Delta u_{\rm p}$ and D for the P2 wave are required to calculate the final Hugoniont stress (peak stress) and volume of the shock experiment. The $\Delta u_{\rm p}$ is simply $(u_{\rm imp} - u_{\rm S1})/2$, where $u_{\rm imp}$ is the impact velocity. In order to obtain D for the P2 wave, we refer to the h, t diagram of Figs. 3 and 4. Let the velocity of the reflected P1 wave (R1) be equal to the velocity of incident P1 wave. In addition, from Eq. (5) the velocity of the residue of the P2 wave ($\rm P2^R$) is known. Thus, knowing these two wave velocities and the times t_1 and t_3, one can calculate the wave interaction coordinates (h_2, t_2). The desired Lagrangian shock velocity of the P2 wave is then simply $D = h_2/t_2$. Therefore, the change in stress and volume carried by the P2 wave can be calculated from Eq. (4). In this case, the shock peak stress and volume could be obtained. The results are also listed in Table 3.

Next, we now wish to calculate the stress $\sigma_{\rm r}$ and particle velocity immediately behind the residue of the P2 wave ($\rm P2^R$). When the residue of the P2 wave reaches the free surface, the free surface velocity increases from $u_{\rm S1}$ to $u_{\rm S3}$. Using the factor-of-2 approximation, the particle velocity behind the $\rm P2^R$ wave is $u_{\rm p} = (u_{\rm S1} + u_{\rm S3})/2$, and the change in particle velocity carried by the wave is $\Delta u_{\rm p} = (u_{\rm S3} - u_{\rm S1})/2$. As discussed previously, the $\rm P2^R$ wave travels in purely α-phase, and we assume D is known as the Eq. (5) of $u_{\rm p}$ for α pure iron or FeMnNi alloy. Thus, both D and $\Delta u_{\rm p}$ for the $\rm P2^R$ wave are known, and the stress behind the $\rm P2^R$ wave, $\sigma_{\rm r}$, can be found from Eq. (4). The results are also listed in Table 3. Both stress and particle velocity are continuous across interface boundaries. Therefore, the same stress and particle velocity exist in the sample to the left of the interface at h_2.

Therefore, for the pure iron sample in experiment No.1, the stress behind the $\rm P2^R$ wave, $\sigma_{\rm r} = 2.5$ GPa, is not only less than the stress ($\sigma_{\rm n} = 9.8$ GPa) below which the reverse phase transition $\varepsilon \to \alpha$ begins, but also less than the stress (about 5.5 GPa) below which the reverse phase transition $\varepsilon \to \alpha$ ends.[2] Thus under release process, in the pure iron sample to the left of the interface at h_2 the $\varepsilon \to \alpha$ reverse phase transition has entirely completed. This material's stress–volume release path must be much less steep than the stress–volume release path for the α material in order to accomplish the now mandatory reverse phase transition, and it produces the rarefaction shock wave (RSW). The phase structure is α phase behind the RSW (see Fig. 3). The unloading profile may present three wave structures consisting of the rarefaction wave $\rm R1^R$ and the rarefaction shock wave RSW and the rarefaction wave R2.

In order to study the unloading process of the FeMnNi sample in experiment No. 3, the reverse phase transition stress of FeMnNi is required to obtain through the reverse impact experiment No. 4. The interface velocity of the flyer/window in the reverse impact test No. 4 is shown in Fig. 5. From the parameters of the sapphire window in Table 1 and the first part of Eq. (4) and Eq. (5), we obtained the shock peak stress in this test is about 11.3 GPa, which is much higher than that of the phase transition for FeMnNi (6.3 GPa). The shock peak stress in experiment No. 4 is almost equal to that in experiment No. 3, and thus the stress wave structure of the flyer in experiment No. 4 is assumed to be in according with that of the sample in experiment No. 3. Referring to

Fig. 4, under shock compression, the FeMnNi flyer in experiment No. 4 starts from α phase, and then after elastic and plastic waves it transforms to the ε phase or $\alpha+\varepsilon$ mixed phase via the phase transition wave P2. However, at the impact surface they do not split and will be assigned by VISAR as a single wave. Under release process, the left going plastic wave P1 reflects at the rear side of the flyer and travels as a rarefaction wave R1 back into the flyer, and it encounters the oncoming phase transition wave P2, then the pressure in the FeMnNi flyer begins to low down. This change may induce the particle velocity at the interface of the flyer/window variation and the rarefaction wave R will be measured by VISAR. Further more, the residue of the P2 wave will run forward continuing until it interacts with the rear side of the flyer. The reflection of the residue phase transition wave $P2^R$ will produce another rarefaction wave in the flyer, which induces the flyer/window interface velocity to drop suddenly. This drop is called the RSW in many early literatures and measured in this study for FeMnNi alloy. Referring to Fig.5, the stress of the reverse phase transition in FeMnNi alloy, $\sigma_n = 4.2$ GPa, is obtained from the first part of Eq. (4), Eq. (5), and the parameters of the sapphire window.

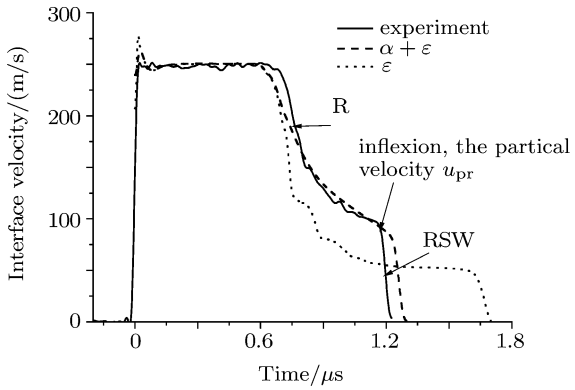


Fig. 5. Experimental and simulation of the flyer/window interface velocity in experiment No. 4. Solid line—experiment signal by means of VISAR, dot line—Case 1 ε phase after the P2 wave, dash line—Case 2 $\alpha+\varepsilon$ phase after after the P2 wave. u_{pr} is the interface particle velocity at which the reverse phase transition begins.

Therefore, referring to Fig. 4, in experiment No. 3, the stress behind the $P2^R$ wave, σ_r, is higher than the reverse phase transition stress of FeMnNi, σ_n. In this case, the material in FeMnNi sample to the left of the interface at h_2 has not occurred $\varepsilon \to \alpha$ reverse phase transition, and the phase structure remains ε phase or $\alpha+\varepsilon$ mixed phase after the rarefaction wave $R1^R$. There will exist, after time t_2, a phase interface at h_2 between the α and ε phase (or the $\alpha+\varepsilon$ mixed phase). At time t_3, the $P2^R$ wave reaches and reflects from the free surface as a rarefaction wave R2. At time t_4, the rarefaction wave R2 arrivals at the phase interface at h_2, and the release wave $R2^R$ enters into the ε phase or the $\alpha+\varepsilon$ mixed phase. However, there is a mismatch of material properties at h_2, and thus the rarefaction wave R2 is reflected back toward the free surface as a recompression, and produces the PIR wave. Since the wave velocities in α phase of FeMnNi alloy do not vary drastically with stress level or loading direction, it is seen from Fig. 4 that the phase interface reflection (PIR wave) should arrive at the free surface at a time roughly equal to $t_5 = t_3 + (t_3 - t_1)$, with a free surface velocity of u_{S5}. This time agrees with the experimentally observed arrival time of the final increase in the free surface velocity profile. The particle velocity behind the PIR wave is $u_p = (u_{S3}+u_{S5})/2$, and the change in particle velocity is $\Delta u_p = (u_{S5}-u_{S3})/2$. Using Δu_p and the known properties of α phase FeMnNi alloy, D is obtained from Eq. (5) and the stress behind the PIR wave, σ_s, is found from Eq. (4). Since the properties of both stress and particle velocity are continuous, the same stress and particle velocity exist in the FeMnNi sample to the left of the interface at h_2. The stress behind the PIR wave, $\sigma_s = 0.3$ GPa, is little, and it is obviously less than the reverse phase transition stress, σ_n. Therefore, as the release wave $R2^R$ enters into the FeMnNi sample to the left of the interface at h_2, the ε phase or the $\alpha+\varepsilon$ mixed phase material will transform to the α phase, and it produces the RSW. Recall also, we have obtained the rarefaction wave $R1^R$ and $R2^R$, and thus the unloading profile may present three wave structure consisting of the rarefaction wave $R1^R$ and the rarefaction wave $R2^R$ and the RSW. However, $R1^R$ and $R2^R$ are difficult to distinguish from the experimental observation, and thus the two wave structure consisting of the rarefaction wave R and the RSW is registered in the reverse impact experiment No. 4.

For the pure iron sample in experiment No. 1, the shock peak stress 14.8 GPa is higher than the phase transition stress 13 GPa, but less than the stress (about 20 GPa)[2,20] at which the α phase transforms almost to the ε phase entirely in pure iron. Thus the phase state of the pure iron sample in experiment No.1 is metastable mixed phase $\alpha+\varepsilon$ after P2 wave (see Fig. 3). In addition, due to the absence of the stress

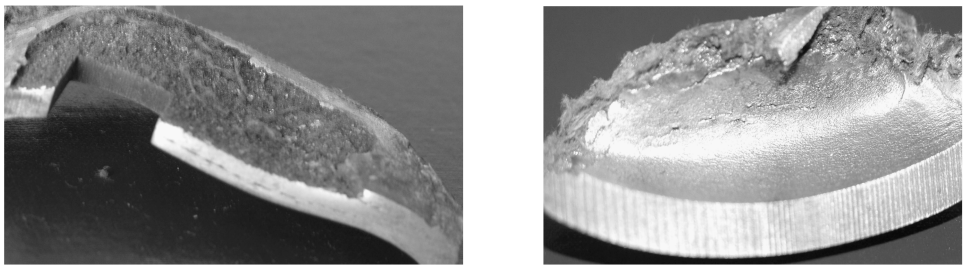
at which the α phase transforms to the ε phase entirely in FeMnNi alloy, we studied the phase state of FeMnNi alloy after P2 wave in experiments No. 3 and No. 4 through the numerical simulation based on the phase transformation model (see section 3). Parameters of the model were chosen from experimental stress wave profile. Figure 5 shows the results of the numerical simulation. Two cases are computed and compared with the experimental measurements. In case 1, it is assumed that the phase state of FeMnNi alloy after P2 wave is the single ε high pressure phase. It can be seen that the numerical simulation of case 1 is markedly different from the experimental result. Therefore, we propose that case 1 does not fit this study. For the second case, it is assumed that the phase state of FeMnNi alloy after P2 wave is the metastable mixed phase $\alpha + \varepsilon$. The simulation result of this case is basically in agreement with the experiment very well. Therefore, the phase state of FeMnNi alloy after P2 wave in experiments No. 3 and No. 4 is the metastable mixed phase $\alpha + \varepsilon$.

4.2. Spalling characteristics

Figure 6 shows the recovered samples in experiment No. 1 and No. 2. In experiment No. 2, spalling does not happen in the sample. While in experiment No.1 there are two spalls occurred in the recovered sample: one complete fracture is located at about 2 mm from the free surface and another incomplete fracture is located at about 2 mm from the impact surface. The result from the recovered samples is in accordance with the analytical result from the free surface velocity. The width of the spall piece δ can be obtained from the free surface velocity profiles in Fig. 2 through Eq. (6).

$$\delta = C_{\mathrm{L}} \times T/2, \tag{6}$$

where C_{L} is the Lagrange sound speed; T is the oscillation period at the free surface velocity profile.



(a) (b)

Fig. 6. (a) Two spallation positions on the cross-section of the recovered sample in experiment No.1; (b) The recovered sample with the whole impact surface and the whole free surface in experiment No. 2.

According to the stress theory, spall will not happen in general case for the symmetrical and same-thickness impact such as experiment No. 2. However, the double spalling occurs in experiment No. 1, and the big physical difference is the $\alpha - \varepsilon$ phase transition comparing with the experiment No. 2. Hence, this abnormal spalling phenomenon in experiment No. 1 might be related to the phase transition. The physical process in experiment No. 1 is described in Fig. 7. The wave structures in the flyer and in the sample are symmetrical along the impact surface. Due to the low magnitude of the elastic wave, it has been omitted in Fig. 7. The plastic shock wave P1 interacts with the free surface of the sample and travels back into the sample as a rarefaction wave R1. The rarefaction wave R1 encounters the oncoming phase transition wave P2, then travels back into $\alpha + \varepsilon$ mixed phase as a rarefaction wave $\mathrm{R1^R}$. The $\alpha + \varepsilon$ mixed phase transforms into α phase, and it produces RSW. The residue of the P2 wave ($\mathrm{P2^R}$) reaches and reflects at the sample free surface, and it travels back into the sample as an another rarefaction wave R2. Further more, the RSW collides with $\mathrm{RSW^f}$ from the back free surface of the flyer, and the first tension region TR1 comes into being, which causes the incomplete spall near the impact surface. The interaction between the rarefaction wave R2 and the residue of the right rarefaction wave through the first tension region induces the second tension region TR2, which causes the complete spall near the free surface.

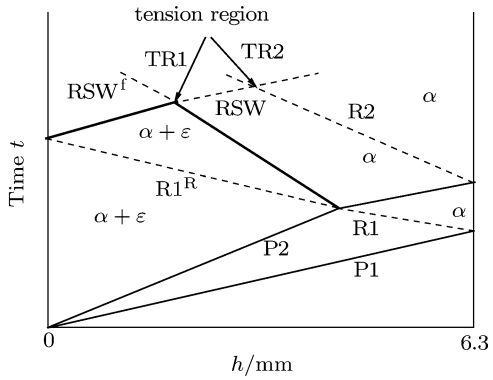


Fig. 7. Stress wave interaction schematic diagram of the pure iron sample in experiment No.1, in which the horizontal axis represents the sample thickness, the left end represents the impact surface, and the right end represents the free surface.

In addition, we described the physical process in experiment No. 3 through the numerical simulation method, and the results were shown in Figs. 2 and 8. From Fig. 2 it can be seen that the numerical simulation is in good agreement with the experimental result, and no complete spallation occurs in the sample. However, Fig. 8 indicates clearly that there are two tensile spall regions in the sample. The possible reason is that the tension stress induced by the unloading wave is less than that of the spalling strength of the FeMnNi sample. The wave structures in the flyer and in the sample are symmetrical along the impact surface. The plastic shock wave P1 interacts with the free surface of the sample and travels back into the sample as a rarefaction wave R1. The rarefaction wave R1 collides with the oncoming phase transition wave P2, and then travels back into $\alpha+\varepsilon$ mixed phase as a rarefaction wave R1$^{\mathrm{R}}$ and lowers the pressure. The residue of the P2 wave (P2$^{\mathrm{R}}$) reaches and reflects at the sample free surface, and it travels back into the sample as an another rarefaction wave R2. When the rarefaction wave R2 arrives at the phase interface at h_2, the release wave R2$^{\mathrm{R}}$ enters into the $\alpha+\varepsilon$ mixed phase. The metastable $\alpha+\varepsilon$ mixed phase transforms into the α phase, and it produces the RSW. Further more, the rarefaction wave R2$^{\mathrm{R}}$ collides with the reflecting RSW$^{\mathrm{f}}$ from the back free surface of the FeMnNi flyer, and the first tension region TR1 comes into being. The interaction between the RSW and the residue of the right rarefaction wave through the first tension region induces the second tension region TR2.

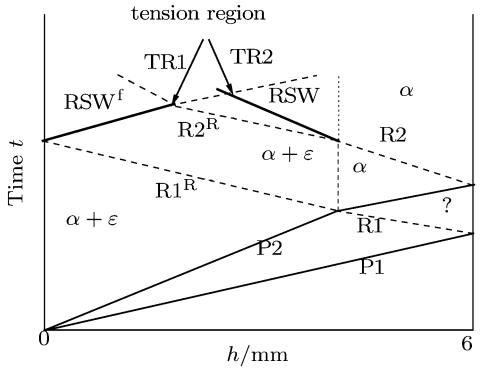


Fig. 8. Stress wave interaction schematic diagram of the FeMnNi sample in experiment No. 3, in which the horizontal axis represents the sample thickness, the left end represents the impact surface, and the right end represents the free surface.

5. Conclusions

The $\alpha-\varepsilon$ phase transition and spalling behaviours of pure iron and FeMnNi alloy were investigated under different impact pressures through experiments and numerical simulations. It is found that the loading and unloading processes present an obvious difference in pure iron and FeMnNi alloy because of the different impact pressure and the reverse phase transition stresses. However, the results indicate that the phase transition affects consumingly spalling behaviour in either pure iron or FeMnNi alloy.

For pure iron, the symmetric and same-thickness impact produces an abnormal multiple spalling. The abnormal spalling phenomenon is believed to relate to the $\alpha-\varepsilon$ phase transition of pure iron, and a possible reason for the abnormal spalling is discussed also from the interaction process of stress wave.

For FeMnNi alloy, the loading and unloading processes were explored by both experimental investigation and numerical simulation. The results show that in the loading process, FeMnNi alloy experiences $\alpha-\varepsilon$ phase transformation and the phase transition pressure is about 6.3 GPa. However, the ε phase is not stable and it will transform to the α phase during the unloading process below the stress of around 4.2 GP. And the influence of the shock-induced phase transition on the spalling behaviour of FeMnNi alloy is explained well.

References

[1] Bancroft D, Peterson E and Minshall S 1956 *J. Appl. Phys.* **27** 291

[2] Barker L M and Hollenbach R E 1974 *J. Appl. Phys.* **45** 4872

[3] Shockey D A, Curran D R and de Carli P S 1975 *J. Appl. Phys.* **46** 3766

[4] Veeser L R, Gray G T, Vorthman J E, Rodriguez P J, Hixson R S and Hayes D B 1999 *Shock Compression of Condensed Matter* 73

[5] Christophe V and Gilles R 2003 *Shock Compression of Condensed Matter* 511

[6] Christophe V, Francois B and Gilles R 2005 *Shock Compression of Condensed Matter* 678

[7] Tang Z P, Tang X J, Zhang X H, Hu H B and Xu W W 2005 *Shock Compression of Condensed Matter* 662

[8] Zhu Z Y, Wang W Q and Liu G D 2005 *Acta Phys. Sin.* **54** 4909 (in Chinese)

[9] Zheng H X, Liu J, Xia M X and Li J G 2005 *Acta Phys. Sin.* **54** 1719 (in Chinese)

[10] Cui X L, Zhu W J, Deng X L, Li Y J and He H L 2006 *Acta Phys. Sin.* **55** 5545 (in Chinese)

[11] Shao J L, Wang P, Qin C S and Zhou H Q 2008 *Acta Phys. Sin.* **57** 1254 (in Chinese)

[12] Shao J L, Wang P, Qin C S and Zhou H Q 2007 *Acta Phys. Sin.* **56** 5389 (in Chinese)

[13] Shao J L, Wang P and Qin C S 2009 *Acta Phys. Sin.* **58** 1936 (in Chinese)

[14] Hawreliak J, Colvin J D and Eggert J H 2006 *Phys. Rev.* B **74** 184107

[15] Hawreliak J, Butterfield M, Huw D, Daniel K and Giles K 2007 *Shock Compression of Condensed Matter* 1327

[16] Zhang X H, Tang Z P and Xu W W 2007 *Explosion and Shock Waves* **27** 103 (in Chinese)

[17] Chen Y T, Hu H B, Tang X J, Li Q Z, Peng Q X and Hu J B 2007 *Shock Compression of Condensed Matter* 493

[18] Boettger J C and Wallace D C 1997 *Phys. Rev.* B **55** 2840

[19] Andrews D J 1971 *J. Comp. Phys.* **7** 310

[20] Hayes D B 1974 *J. Appl. Phys.* **45** 1208